Coaxial ZnSe/Si nanocables with controlled p-type shell doping

To cite this article: Li Wang *et al* 2010 *Nanotechnology* **21** 285206

Nanotechnology **21** (2010) 285206 (7pp) doi:10.1088/0957-4484/21/28/285206

Coaxial ZnSe/Si nanocables with controlled p-type shell doping

Li Wang[1], Jiansheng Jie[1,3], Chunyan Wu[1], Zhi Wang[1], Yongqiang Yu[1,2], Qiang Peng[1], Xiwei Zhang[1], Zhizhong Hu[1], Di Wu[2], Huier Guo[1] and Yang Jiang[2]

[1] School of Electronic Science and Applied Physics, Hefei University of Technology, Hefei Anhui, 230009, People's Republic of China
[2] School of Materials Science and Engineering, Hefei University of Technology, Hefei Anhui, 230009, People's Republic of China

E-mail: jason.jsjie@gmail.com

Received 28 April 2010, in final form 26 May 2010
Published 28 June 2010
Online at stacks.iop.org/Nano/21/285206

Abstract
Coaxial ZnSe/Si nanocables were successfully produced by a simple two-step growth method. ZnSe nanowire cores were first synthesized by thermal evaporation and then followed by the chemical vapor deposition (CVD) growth of Si shells. The former have a cubic single-crystal structure with a longitudinal direction of $[\bar{1}1\bar{1}]$, while the latter are polycrystalline and composed of a large number of Si crystal grains with dominantly (111) surfaces. Controlled p-type doping to the Si shells was implemented by B diffusion after the shell growth. Electrical measurements on the Si shells demonstrated that the shell conductivity could be tuned in a wide range of eight orders of magnitude by adjusting the B concentration, and a hole mobility of 11.7 $cm^2\ V^{-1}\ s^{-1}$ and a hole concentration of $2 \times 10^{15}\ cm^{-3}$ were revealed for the modestly doped Si shells. The ZnSe/Si core/shell nanocables have great potential in nano-optoelectronic applications.

(Some figures in this article are in colour only in the electronic version)

1. Introduction

Nano-heterostructures have emerged as an important class of nanomaterials for diverse applications in nano-photonics and nano-optoelectronics. Different from the conventional nanowires, nanoribbons, and nanotubes, which have homogeneous compositions and structures [1–3], nano-heterostructures consist of two or more kinds of nanomaterials with distinct compositions, conduction types, energy bands, or structures, and have much more important applications as compared with the homogeneous nanostructures due to the existence of junctions. For instance, efficient nanoscale light emission diodes (nanoLEDs) can be formed by crossing p-Si nanowires with other n-type nanowires [4–6], and were realized in InP/InAsP longitudinal and InGaN/GaN coaxial nano-heterostructures [7, 8]. Recently, functional photovoltaic (PV) devices were fabricated from coaxial p–i–n silicon, n-GaN/i-$In_xGa_{1-x}N$/p-GaN, and ZnO/TiO_2 nanowires, and these nanoPV devices have shown high energy conversion efficiencies [9–11].

II–VI group materials, which have direct bandgaps spanning the entire visible spectra, offers an opportunity for developing the next generation of nanowire based electronic and optical components [12]. However, the practical applications of II–VI materials are still hindered by the difficulty in achieving complemental doping with both n- and p-type conduction [13–15]. On the other hand, silicon, an indirect bandgap semiconductor (∼1.12 eV), is of special interest due to its key role in the modern semiconductor industry, and the electrical properties of Si can be readily controlled by efficient doping. Nevertheless, the low emission efficiency caused by the indirect bandgap obstructs its applications in light emission devices. By combining it with II–VI nanostructures, II–VI/Si nano-heterostructures may offer an alternative way to realize Si-based optoelectronic integration.

So far, nano-optoelectronic devices based on II–VI/Si nano-heterostructures have normally been fabricated from a

[3] Author to whom any correspondence should be addressed.

variety of crossed-nanowire junctions, in which p–n junctions were formed by mechanical contact instead of the epitaxial growth in film technique [4–6]. However, such structures are likely plagued with non-idealities arising from interfacial oxides and defects. The most efficient alternative could be constructing nano-optoelectronic devices based on coaxial II–VI/Si core/shell nanocables, in which there are epitaxially formed junctions occurring uniformly over the entire cross section of the nanowire [16]. Also, in this structure, the carriers would be injected along the length of the II–VI cavity from the Si shell, thus high density injection could be achieved, allowing laser emission from II–VI/Si nanocables. To date, most previous research has focused on the synthesis and structure characterizations of coaxial II–VI/Si nanocables, such as CdS/Si, ZnS/Si [17, 18]; there has been only limited research devoted to the control of the growth and doping in such a structure for optoelectronic applications.

Zinc selenide (ZnSe), an important II–VI compound semiconductor with a wide direct bandgap of ∼2.7 eV at room temperature, is the most promising material for blue-light-emitting devices. In fact, the first blue-green laser diodes in world were developed from ZnSe in 1991 [19], which is about five years earlier than the demonstration of GaN-based blue laser diode (early 1996) [20]. In addition, ZnSe has a residual n-type doping in the 0.5–1 × 10^{15} cm^{-3} range and can be easily n-type doped with n-type dopants such as Al and Cl [21]. Efficient p-type doping was also demonstrated in films with N dopant and in nanowires with As dopant [22, 23]. Moreover, ZnSe has a small lattice mismatch of ∼4% with Si, implying a high quality heterojunction would be likely formed at the ZnSe/Si interface.

In this paper, we present a systematic study on preparing coaxial ZnSe/Si core/shell nanocables with controlled p-type doping to the silicon shell. It is expected that the ZnSe/Si nanocables with controlled transport properties have great potential for applications in optoelectronic devices.

2. Experimental details

The synthesis of coaxial ZnSe/Si nanocables was conducted in a horizontal tube furnace via a two-step vapor growth process, and the p-type Si shell doping was accomplished by an additional thermal diffusion process. ZnSe nanowire cores were synthesized first, followed by Si shells deposition. The detailed experimental process can be described as follows: in the first step, ∼0.2 g ZnSe powder (99.99%, Sigma Aldrich) was loaded into an alumina boat and the boat was then transferred to the center region of the furnace. Si substrates, which had been ultrasonically cleaned in acetone and then in alcohol for 10 min, were coated with 10 nm gold catalyst and placed in the downstream position of the ZnSe source at an ∼10 cm distance. The system then was evacuated to a base pressure of 10^{-3} Pa, and backfilled with H_2 (5% in Ar) to a pressure of 300 Torr. The flow rate of the carrier gas was kept at 100 sccm during the growth process. Thereafter, the furnace was heated up to 1040 °C at a rate of 20 °C min^{-1}, and held at this temperature for 2 h. After finishing the growth of the ZnSe nanowires, the furnace was cooled naturally down to room temperature. Bright-yellow colored ZnSe nanowires were observed on the Si substrates. In the second step, an Al_2O_3 boat filled with a boron source (B_2O_3) was located at the center of the tube furnace and the as-synthesized ZnSe nanowires were placed at the downstream position. After evacuating the tube to 10^{-3} Pa, the furnace was heated to 750 °C and maintained at this temperature for 1.5 h. The growth pressure was stabilized at 400 Pa by feeding in a mixed gas flow of 96 sccm H_2 (5% in Ar) and 5 sccm SiH_4 (5% in Ar). Si shells were grown on the ZnSe nanowires during this process. Next, the pressure in the tube was evacuated to 10^{-3} Pa again, and then filled with Ar gas to the pressure at 150 Torr. After that, the furnace was sealed and heated to 900, 950 or 1000 °C, respectively, and kept at that temperature for 30 min for different B doping concentration to the Si shells. Finally, coaxial ZnSe/Si nanocables were fabricated with ZnSe nanowires as the cores and p-Si as the sheaths. In our experiments, three samples with different Si shell doping levels were synthesized, which were marked as SS900, SS950, and SS1000, corresponding to II–VI/p-Si nanocables synthesized at different B diffusion temperatures of 900, 950, and 1000 °C, respectively. Undoped II–VI/Si nanocables were also synthesized for comparison; these were marked as ISS.

As-synthesized samples were characterized by x-ray diffraction (XRD) with Cu Kα radiation (λ = 1.541 78 Å). The morphologies and structures of the samples were investigated by field-emission scanning electron microscopy (FESEM) and transmission electron microscopy (TEM). To assess the electrical properties of the p-Si shells, nanodevices based on single Si shells were constructed. Firstly, the ZnSe nanowire cores were removed by a diluted HCl solution to leave Si shells with tube-like shapes. The tubular Si shells were then dipped into a 5 vol% HF solution for 30 min to remove the outside SiO_2 layer. Afterward, the Si shells were dispersed uniformly onto SiO_2(300 nm)/p^+-Si substrates at a specified density. Photolithography and a following lift-off process were employed to define the source and drain electrodes on a single Si shell. Ti (1.5 nm)/Au (80 nm) double-layer electrodes were used since Au showed the lowest contact resistance to the p-Si shells.

3. Results and discussions

Figure 1(a) shows a typical FESEM image of the coaxial ZnSe/Si nanocables. It is seen that the product has a distinct core–shell structure, and the ZnSe nanowire cores are fully surrounded by silicon shells except the ends (indicated by white arrows). The ZnSe/Si nanocables have lengths of several tens of micrometers and diameters of 200–300 nm. It is noted that the surfaces of the nanocables are smooth and free of impurities and defects, such as particles and pinholes in the shells. Energy dispersive spectroscopy (EDS) reveals the nanocables consist of only Zn, Se, and Si in roughly 26:25:59 atomic ratios (lower-right inset in figure 1(a)). Furthermore, the structures of the coaxial ZnSe/Si nanocables were characterized by XRD measurement, as shown in figure 1(b). All the diffraction peaks in the pattern could be indexed to cubic Si (JCPDS 27-1402) and cubic

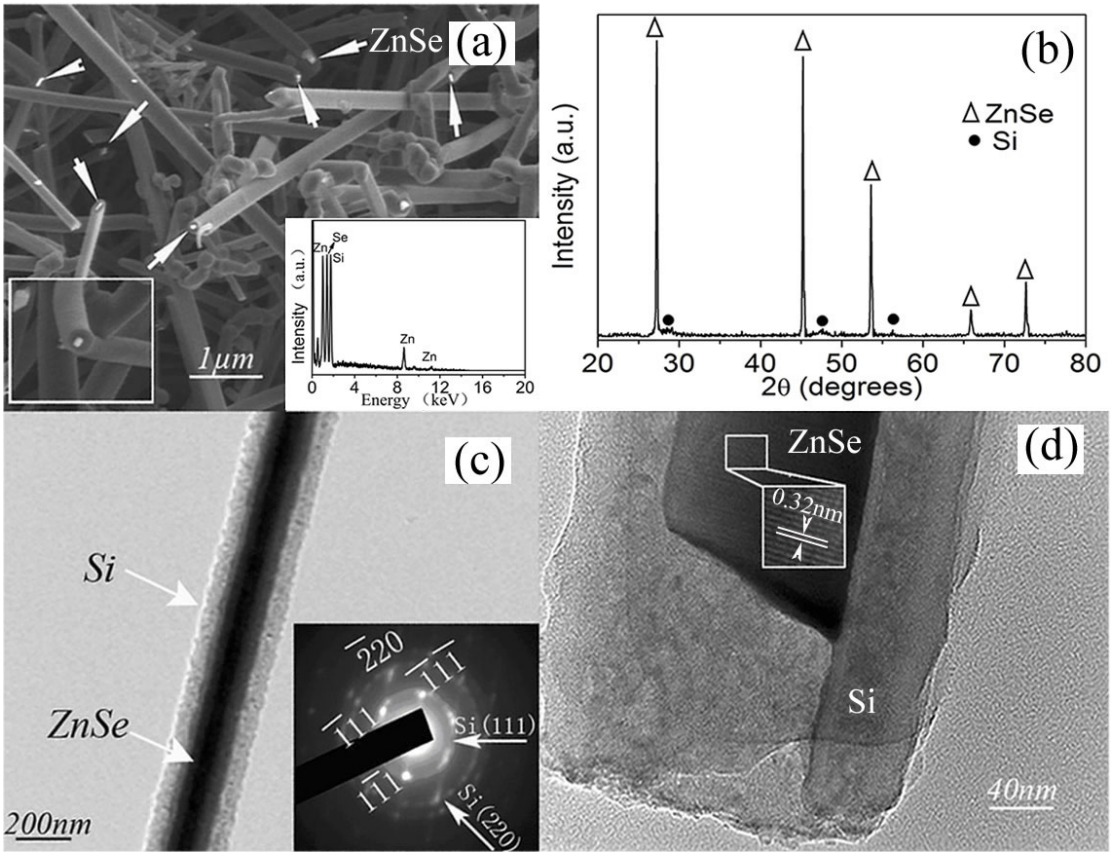

Figure 1. SEM image of the coaxial ZnSe/Si nanocables. The ZnSe cores are indicated by white arrows. The lower-left inset is a magnified SEM image of the top for a coaxial nanocable. The lower-right inset is the EDS spectrum. (b) XRD pattern of the ZnSe/Si nanocables. (c) TEM image of the ZnSe/Si nanocables. The inset shows the corresponding SAED pattern. (d) High-resolution TEM image of a ZnSe/Si nanocable, revealing the single-crystal structure of the ZnSe core.

ZnSe (JCPDS 37-1463) within experimental error, indicating that the as-synthesized nanocables are composed of Si and ZnSe phases. No diffraction peaks from the impurities were detected in the XRD pattern, revealing the high crystalline purity of the product. We note that the peak intensity of Si diffraction is rather low compared with ZnSe, implying a modest crystallinity of the Si shells.

Detailed microstructures of the ZnSe/Si core–shell nanostructures were further investigated using TEM and corresponding selected area electron diffraction (SAED, attached on HRTEM). Figure 1(c) shows a typical low-magnification TEM image of the ZnSe/Si nanocables. The variation of contrast along the radial direction of the nanocable clearly reveals its core/shell structure, in which the light and dark areas correspond to Si shell and ZnSe core, respectively. From the TEM image, the diameter of the ZnSe nanowire cores is around 200–300 nm, and the Si shell thickness is 50–60 nm. It is noted that the core diameter and the shell thickness could be readily controlled by adjusting experimental parameters such as growth temperature and time duration. The inset in figure 1(c) shows the corresponding SAED pattern, in which both diffraction spots and diffraction rings are observed. Analysis of the pattern reveals that the diffraction spots and rings come from the single-crystal ZnSe core and the polycrystalline Si shell, respectively. The single-crystal nature of the ZnSe core is further confirmed by the high-resolution TEM (HRTEM) image in figure 1(d). The lattice spacing of 0.32 nm corresponds to the (111) plane of cubic ZnSe.

To realize high-performance optoelectronic nanodevices based on ZnSe/Si nano-heterostructures, controlled p- and n-type doping to both ZnSe cores and Si shells are essential. In this study, we conducted a primary study on the p-type doping of Si shells using B_2O_3 as the dopant and three samples with different B doping levels were fabricated. To evaluate the effects of the doping, the ZnSe nanowire cores were first removed by diluted HCl solution so that the electrical characterizations could be specified to the outside Si shells. After HCl treatment, tubular Si shells with hollow cavities (could be regarded as Si nanotubes, and we will use the term Si nanotubes instead in the following discussion) were obtained, as shown in figure 2(b) and (c). From the XRD pattern taken from the Si nanotubes (figure 2(a)), only Si diffraction peaks could be observed, implying that the ZnSe cores have been effectively removed and any residual ZnSe is too little to be reflected in the XRD pattern. Further investigation of the TEM images shows that the Si nanotubes have a uniform wall thickness of ∼50 nm, and length of tens of micrometers (figures 2(b) and (c)). It is noted that there are still some black particles on the inside walls of the Si nanotubes, which most likely come from the residual ZnSe

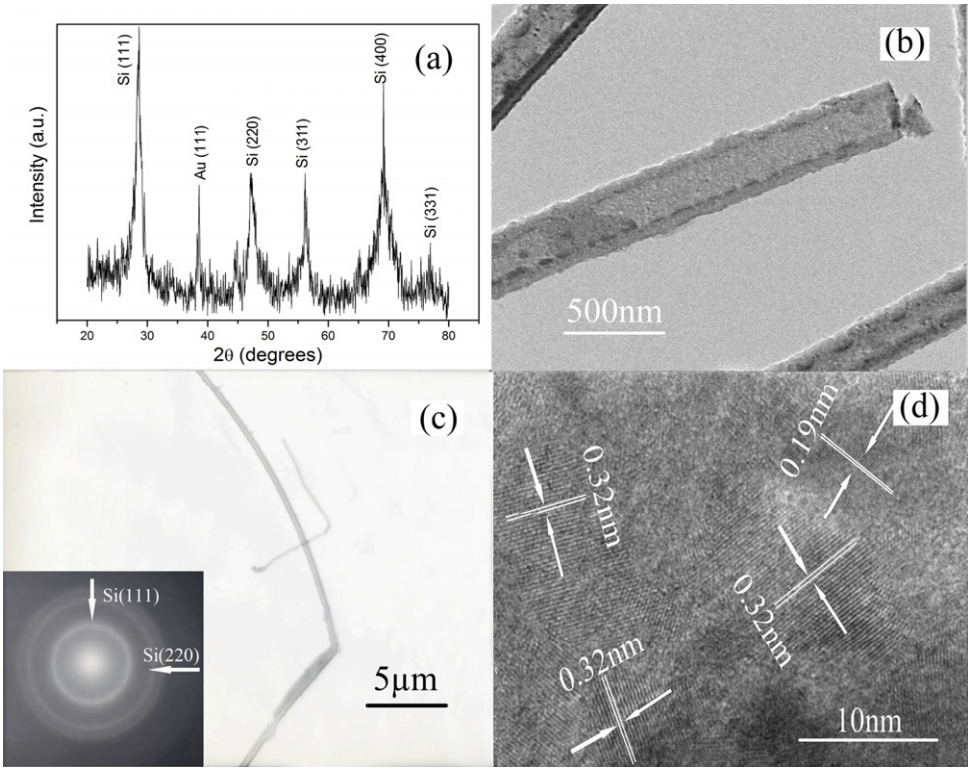

Figure 2. (a) XRD pattern of the sample after treatment with diluted HCl solution. (b) TEM image of the Si shells. (c) A low-resolution TEM image of the Si shells. The inset shows the corresponding SAED pattern. (d) HRTEM image of the Si shells.

cores. Nevertheless, these ZnSe particles are separated from each other and therefore would not have a significant influence on the transport measurements of the Si shells. Moreover, from the SAED pattern taken from a typical Si nanotube (figure 2(c)), there are no observable diffraction spots from ZnSe and the diffraction rings match well with the (111) and (220) planes of Si, confirming that the ZnSe cores have been effectively removed. Figure 2(d) shows the HRTEM image of the Si shell, revealing that the shell is composed of a large number of crystal grains with a nanoscale size of ∼10–15 nm. The lattice spacings of 0.32 nm and 0.19 nm correspond to the (111) and (220) planes of Si, respectively. We note that most of the Si nanograins have (111) surfaces. This is a reasonable result since {111} surfaces have the lowest energy among all of the Si surfaces [24].

Nanodevices based on individual Si nanotubes were constructed to assess the electrical properties of B doped Si shells. Typical I–V curves of the Si nanotubes with varied doping concentration are plotted in figure 3(a), and the inset shows the SEM image of a typical device, in which two parallel electrodes with a separation of 8 μm were deposited on the two ends of the nanotube. Notably, the conductance of these samples is vastly different and strongly dependent on the diffusion temperature of the boron source. The undoped Si shells show the lowest conductivity (around 9.52×10^{-7} S cm^{-1}) among all samples. In contrast, the doped Si shells show enhanced conductivity, which increases to 3.77×10^{-3} S cm^{-1}, 2.43×10^{-1} S cm^{-1}, and 15.7 S cm^{-1} for the samples SS900, SS950, and SS1000, respectively. To have a statistical significance, the conductivity of 20 Si nanotubes was measured for each sample, and the histogram of conductivity is depicted in figure 3(b). The conductivity of undoped Si shells is in the range of $\sim 5.32 \times 10^{-8}$–4.41×10^{-6} S cm^{-1}, whereas the conductivity drastically increases to $\sim 2.62 \times 10^{-3}$–2.14×10^{-2} S cm^{-1} for SS900, $\sim 1.12 \times 10^{-1}$–1.14 S cm^{-1} for SS950, and ∼10–35 S cm^{-1} for SS1000. Significantly, the results suggest that the conductivity of Si shells can be tuned in a wide range of ∼8 orders of magnitude by a simple boron thermal diffusion process. However, the influence of the residual ZnSe core on the conductivity of the Si nanotubes is not fully clear. Nevertheless, we note that the undoped ZnSe is approximately insulating and thus will contribute little to the conductance enhancement of the Si shell. On the other hand, since the same etching process was adopted for all the samples, the influence of residual ZnSe particles, if they have any, to these samples should be the same. Therefore, the change in the conductivity of the Si nanotubes is most likely attributed to the varied B doping concentration but not the effects of residual ZnSe.

Nano-field-effect transistors (nanoFETs) based on single Si nanotubes were fabricated to further study the transport properties of the Si shells (figure 4(a)). Typical gate-dependent source–drain current (I_{ds}) versus source–drain voltage (V_{ds}) curves measured on sample SS900 under varied gate voltage (V_g) from −5 to 5 V are shown in figure 4(b). Significantly, the device shows a pronounced gating effect and I_{ds} increases with decreasing V_g, which is the typical behavior of a p-channel FET. The field-effect hole mobility and hole concentration can be deduced from the electrical characteristics according to the

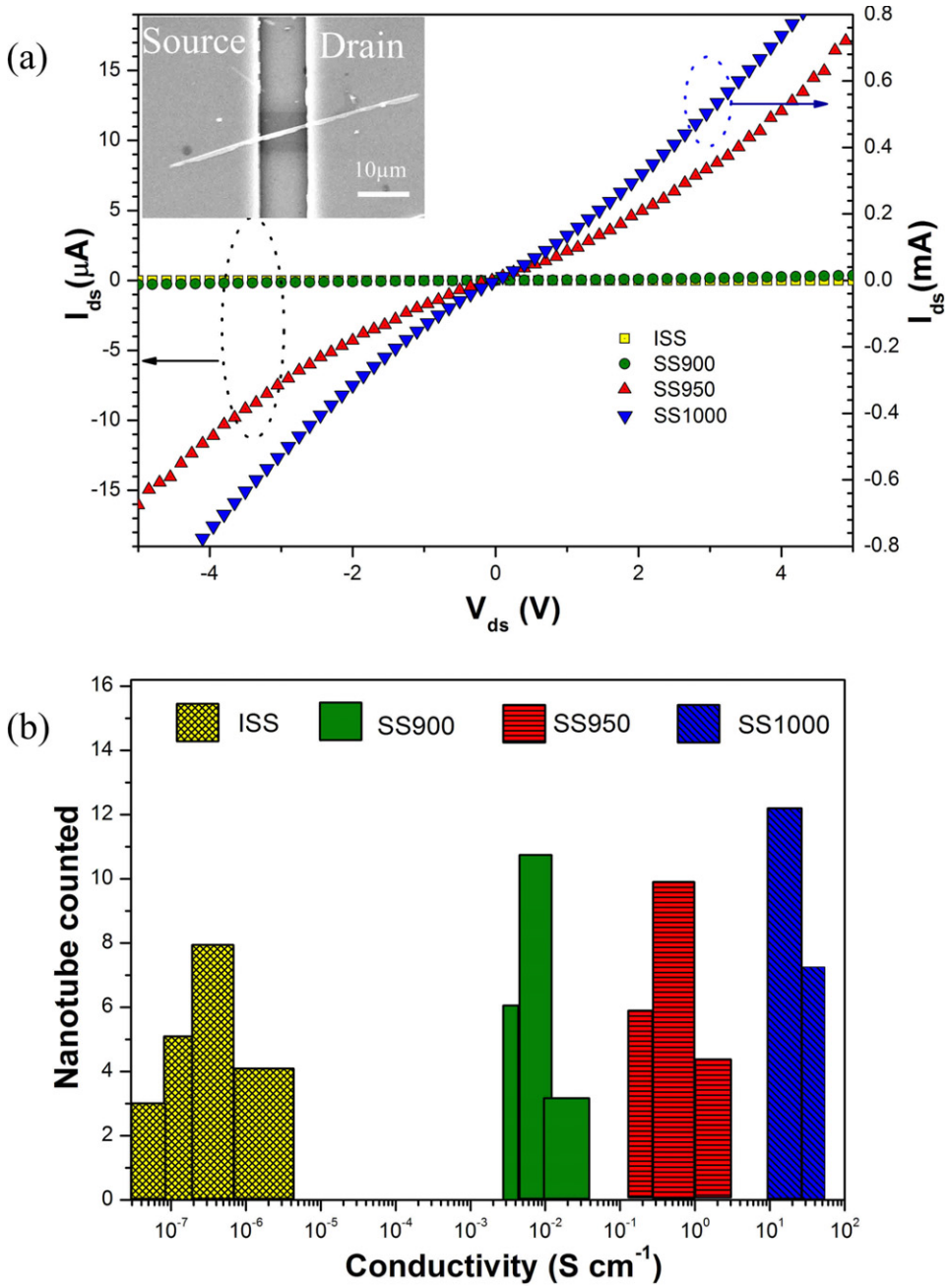

Figure 3. (a) Typical I–V curves of both the intrinsic and doped Si nanotubes measured on individual nanotubes. The inset shows the SEM image of the nanodevice constructed on a single Si nanotube. (b) Distribution of conductivity values for 80 devices, 20 devices each for ISS, SS900, SS950, and SS1000.

following equations as:

$$\mu_{\text{eff}} = \frac{\mathrm{d}I_{\text{ds}}}{\mathrm{d}V_{\text{g}}} \frac{\ln(4h/d)\,L}{2\pi\varepsilon_0\varepsilon_{\text{SiO}_2}} \tag{1}$$

$$n = \sigma/\mu q \tag{2}$$

where the $\mathrm{d}I_{\text{ds}}/\mathrm{d}V_{\text{g}}$ is extracted from the linear region of the transconductance, $\varepsilon_{\text{SiO}_2}$ is the dielectric constant of the SiO_2 gate insulator ($\sim$3.9), L, h, and d represent the Si nanotube channel length, gate oxide layer thickness, and Si nanotube diameter, respectively, n is the carrier concentration, and σ is the conductivity of the Si nanotubes. It is noted that the doped Si shells have a hole mobility of about 11.7 cm^2 V^{-1} s^{-1}, which is close to the value reported before in thin-film transistors (TFT) based on microcrystalline Si [25]. Also, the hole concentration in the Si nanotubes is calculated to be $\sim 2 \times 10^{15}$ cm^{-3} for sample SS900, which is much higher than the value for undoped Si ($\sim 1.45 \times 10^{10}$ cm^{-3}) [26], indicating that the carrier concentration in the Si shells can be increased effectively by the boron doping. Moreover, our results also demonstrate that the coaxial ZnSe/Si nanocables could be a good precursor for the fabrication of Si nanotubes, which are expected to serve as nanoscale containers or pipes to deliver fluids and molecular species, and are excellent building blocks

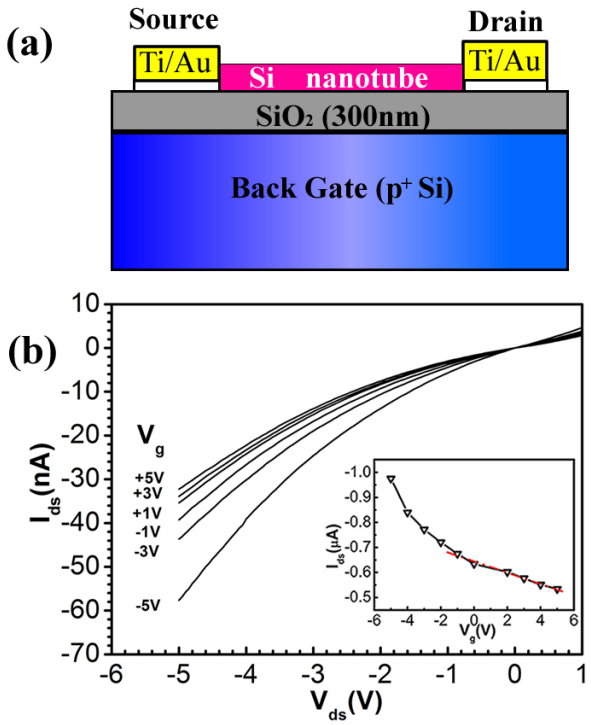

Figure 4. (a) Schematic illustration of the back-gate nanoFET. (b) Transfer characteristics of the nanoFET fabricated from single Si nanotubes (SS900). I_{ds} versus V_{ds} curves were measured under varied V_g ranging from −5 to 5 V. The inset shows the I_{ds} versus V_g curve at $V_{ds} = -0.02$ V. The linear part of the curve was fitted by a line.

for the construction of large-scale nanofluidic systems [27]. Controlled p-type doping to the Si nanotubes offers the possibility to fabricate a variety of novel nanodevices, such as high-sensitivity bio-sensors and ionic liquid nanoFETs [28].

4. Conclusions

In summary, we have successfully fabricated ZnSe/Si core/shell nanocables using a two-step method. The ZnSe nanowire cores were first grown by thermal evaporation via vapor–liquid–solid (VLS) Au catalytic growth, and then a layer of Si shells was deposited on the ZnSe nanowires via a chemical vapor deposition (CVD) process. The ZnSe NW cores have a single-crystal cubic structure with a growth direction of $[\bar{1}1\bar{1}]$ and diameter around 200–300 nm. The Si shells, with thickness 50–60 nm, have a polycrystalline structure, which is made up of a large number of nanoscale crystal grains with a (111) dominating surface. B doping to the Si shells by thermal diffusion results in a remarkable increase in conductivity, which can be tuned in a wide range of eight orders of magnitude by adjusting the doping concentration. FET measurements on a single polycrystalline Si:B nanotube reveal it to be of p-type character, and a hole mobility of ∼11.7 $cm^2\ V^{-1}\ s^{-1}$ and a hole concentration of ∼2 × $10^{15}\ cm^{-3}$ are deduced from the transfer characteristics. It is expected that the coaxial ZnSe/Si nanocables with controlled p-type shell doping have great potential in nano-optoelectronic applications.

Acknowledgments

This work was supported by grants from the National High Technology Research and Development Program of China (no. 2007AA03Z301), the National Natural Science Foundation of China (nos 60806028, 20901021, 20771032), the National Basic Research Program of China (no. 2006CB933000), Fundamental Research Funds for the Central Universities (no. 2010HGXJ0221), and the Program for New Century Excellent Talents in Universities of the Chinese Ministry of Education (NCET-08-0764).

References

[1] Huang M H, Mao S, Feick H, Yan H, Wu Y, Kind H, Weber E, Russo R and Yang P 2001 Room-temperature ultraviolet nanowire nanolasers *Science* **292** 1897–9
[2] Johnson J C, Yan H, Yang P and Saykally R J 2003 Optical cavity effects in ZnO nanowire lasers and waveguides *J. Phys. Chem.* B **107** 8816–28
[3] Zapien J A, Jiang Y, Meng X M, Chen W, Au F C K, Lifshitz Y and Lee S T 2004 Room-temperature single nanoribbon lasers *Appl. Phys. Lett.* **84** 1189–91
[4] Duan X, Huang Y, Cui Y, Wang J and Lieber C M 2001 Indium phosphide nanowires as building blocks for nanoscale electronic and optoelectronic devices *Nature* **409** 66–9
[5] Huang Y, Duan X and Lieber C M 2005 Nanowires for integrated multicolor nanophotonics *Small* **1** 142–7
[6] Zhong Z, Qian F, Wang D and Lieber C M 2003 Synthesis of p-type gallium nitride nanowires for electronic and photonic nanodevices *Nano Lett.* **3** 343–6
[7] Minot E D *et al* 2007 Single quantum dot nanowire LEDs *Nano Lett.* **7** 367–71
[8] Qian F, Li Y, Gradecak S, Wang D, Barrelet C J and Lieber C M 2004 Gallium nitride-based nanowire radial heterostructures for nanophotonics *Nano Lett.* **4** 1975–9
[9] Tian B, Zheng X, Kempa T J, Fang Y, Yu N, Yu G, Huang J and Lieber C M 2007 Coaxial silicon nanowires as solar cells and nanoelectronic power sources *Nature* **449** 885–90
[10] Dong Y, Tian B, Kempa T J and Lieber C M 2009 Coaxial group III-nitride nanowire photovoltaics *Nano Lett.* **9** 2183–7
[11] Law M, Greene L E, Radenovic A, Kuykendall T, Liphardt J and Yang P 2006 ZnO–Al_2O_3 and ZnO–TiO_2 core–shell nanowire dye-sensitized solar cells *J. Phys. Chem.* B **110** 22652–63
[12] Zapien J A, Liu Y K, Shan Y Y, Tang H, Lee C L and Lee S T 2007 Continuous near-infrared-to-ultraviolet lasing from II–VI nanoribbons *Appl. Phys. Lett.* **90** 213114
[13] Park R M, Troffer M B, Rouleau C M, DePuydt J M and Haase M A 1990 p-type ZnSe by nitrogen atom beam doping during molecular beam epitaxial growth *Appl. Phys. Lett.* **57** 2127
[14] Qiu J, DePuydt J M, Cheng H and Haase M A 1991 Heavily doped p-ZnSe:N grown by molecular beam epitaxy *Appl. Phys. Lett.* **59** 2992
[15] Ohkawa K, Karasawa T and Mitsuyu T 1991 Characteristics of p-type ZnSe layers grown by molecular beam epitaxy with radical doping *Japan. J. Appl. Phys.* **30** L152–5
[16] Motayed A and Davydov A V 2008 GaN-nanowire/amorphous-Si core–shell heterojunction diodes *Appl. Phys. Lett.* **93** 193102
[17] Li Q and Wang C R 2003 One-step fabrication of uniform Si-core/CdSe-sheath nanocables *J. Am. Chem. Soc.* **125** 9892–3
[18] Chen Z H, Tang H, Fan X, Jie J S, Lee C S and Lee S T 2008 Epitaxial ZnS/Si core–shell nanowires and single-crystal silicon tube field-effect transistors *J. Cryst. Growth* **310** 165–70

[19] Hasse M, Qui J, DePuydt J and Cheng H 1991 Short wavelength II–VI laser diodes *Appl. Phys. Lett.* **59** 1272–4
[20] Nakamura S, Senoh M, Nagahama S, Iwasa N, Yamada T, Matsushita T, Kiyoku H and Sugimoto Y 1996 InGaN-based multi-quantum well structure laser diodes *Japan. J. Appl. Phys.* **35** L174–8
[21] Monroy E, Omnès F and Calle F 2003 Wide-bandgap semiconductor ultraviolet photodetectors *Semicond. Sci. Technol.* **18** R33–51
[22] Boo B H, Xu N and Lee J K 2002 Growth of crystalline ZnSe:N thin films by pulsed laser ablation deposition *Vacuum* **64** 145–51
[23] Song H S, Zhang W J, Yuan G D, He Z B, Zhang W F, Tang Y B, Luo L B, Lee C S, Bello I and Lee S T 2009 p-type conduction in arsenic-doped ZnSe nanowires *Appl. Phys. Lett.* **95** 033117
[24] Chen Y W, Tang Y H, Pei L Z and Guo C 2005 Self-assembled silicon nanotubes grown from silicon monoxide *Adv. Mater.* **17** 564–7
[25] Krishnan A T, Bae S and Fonash S J 2001 Fabrication of microcrystalline silicon TFTs using a high-density plasma approach *IEEE Electron Device Lett.* **22** 399–401
[26] Sze S M and Kwok N K 2007 *Physics of Semiconductor Devices* 3rd edn (New York: Wiley) p 617
[27] Ishai M B and Patolsky F 2009 Shape- and dimension-controlled single-crystalline silicon and SiGe nanotubes: toward nanofluidic FET devices *J. Am. Chem. Soc.* **131** 3679–89
[28] Karnik R, Fan R, Yue M, Li D, Yang P and Majumdar A 2005 Electrostatic control of ions and molecules in nanofluidic transistors *Nano Lett.* **5** 943–8